EML3 is a nuclear microtubule-binding protein required for the correct alignment of chromosomes in metaphase

Justus Tegha-Dunghu[1], Beate Neumann[2], Simone Reber[1], Roland Krause[3], Holger Erfle[2], Thomas Walter[2], Michael Held[2], Phill Rogers[2], Kerstin Hupfeld[1], Thomas Ruppert[1], Jan Ellenberg[2] and Oliver J. Gruss[1,*]

[1]Zentrum für Molekulare Biologie der Universität Heidelberg (ZMBH), Im Neuenheimer Feld 282, 69120 Heidelberg, Germany
[2]MitoCheck Project Group, European Molecular Biology Laboratory, Meyerhofstr.1, 69117 Heidelberg, Germany
[3]Max-Planck-Institut für Molekulare Genetik, Ihnestr. 73, 14195 Berlin, Germany
*Author for correspondence (e-mail: o.gruss@zmbh.uni-heidelberg.de)

Accepted 28 February 2008
Journal of Cell Science 121, 1718-1726 Published by The Company of Biologists 2008
doi:10.1242/jcs.019174

Summary

Assembly of the mitotic spindle requires a global change in the activity and constitution of the microtubule-binding-protein array at mitotic onset. An important subset of mitotic microtubule-binding proteins localises to the nucleus in interphase and essentially contributes to spindle formation and function after nuclear envelope breakdown. Here, we used a proteomic approach to selectively identify proteins of this category and revealed 50 poorly characterised human gene products, among them the echinoderm microtubule-associated-protein-like gene product, EML3. Indirect immunofluorescence showed that EML3 colocalises with spindle microtubules throughout all mitotic stages. In interphase, EML3 colocalised with cytoplasmic microtubules and accumulated in interphase nuclei. Using YFP-fusion constructs of EML3, we located a nuclear localisation signal and confirmed the microtubule-binding domain of EML3. Functional analysis of EML3 using time-lapse fluorescence microscopy and detailed end-point analysis of phenotypes after siRNA knockdown demonstrates an important role for EML3 in correct metaphase chromosome alignment. Our proteomic identification screen combined with sensitive phenotypic analysis therefore provides a reliable platform for the identification and characterisation of proteins important for correct cell division.

Supplementary material available online at
http://jcs.biologists.org/cgi/content/full/121/10/1718/DC1

Key words: Spindle proteins, Nuclear Proteins, EML3

Introduction

Stable inheritance of genetic information relies on correct assembly of the mitotic spindle, which segregates sister chromatids into two identical sets. Defects in spindle function can lead to genomic instability, which is a hallmark of human cancer. To build up the spindle and to mediate its function in chromosome segregation, numerous microtubule-associated proteins (MAPs) and molecular motors functionally influence microtubule dynamics, microtubule organisation and interaction of microtubules with chromosomes (for reviews, see Kops et al., 2005; Compton, 2000; Wittmann et al., 2001; Cassimeris and Skibbens, 2003; Gadde and Heald, 2004; Kline-Smith and Walczak, 2004).

In higher eukaryotes, spindles form after breakdown of the nuclear envelope and endogenous membrane structures (open mitosis). Many proteins with essential functions in spindle formation are only recruited after reorganisation of these compartments. Consistently with this, a number of spindle proteins are nuclear proteins during interphase. Among them are MAPs such as TPX2 or PRC1, which locate to the nucleoplasm in interphase. The importance of nuclear proteins for spindle assembly has been highlighted by experiments in cell-free extracts of *Xenopus* eggs. In this system, the addition of RanGTP triggers the assembly of spindle-like structures. RanGTP releases nuclear proteins from bound importins and activates them. Several target proteins of RanGTP could be identified by functional assays (for reviews, see Dasso, 2002; Di Fiore et al., 2004; Gruss and Vernos, 2004). Moreover, recent experiments have demonstrated that RanGTP is essential for spindle formation in *Caenorhabditis elegans* (Askjaer et al., 2002; Bamba et al., 2002) and *Drosophila melanogaster* embryos (Silverman-Gavrila and Wilde, 2006), suggesting that the recruitment of proteins from the dissolving nucleus to the spindle is an important general principle in spindle formation of higher eukaryotes.

Since MAPs and motors influence microtubule behaviour by direct binding, identification of spindle-associated proteins is essential to understand spindle structure and function. Several approaches have previously identified microtubule-binding proteins on a proteomic basis in human (Mack and Compton, 2001) and even in *Xenopus* cell-free extracts (Liska et al., 2004). Recently, Sauer et al. purified complete spindle structures from human somatic cells and listed 795 proteins that associated with spindles. They identified several poorly characterised human gene products as spindle components (Sauer et al., 2005).

Here, we specifically analysed the fraction of proteins that both co-fractionate with interphase nuclei of human somatic cells and also co-sediment with microtubules. The proteomic survey of this fraction identified a large number of proteins with known functions as well as 50 poorly characterised human gene products. We further analysed one identified gene product, the echinoderm microtubule-associated protein like 3, EML3 (also known as EMAP3 and

EMAP95). Indirect immunofluorescence and visualisation of YFP fusions demonstrate spindle localisation of EML3 and small interfering RNA (siRNA) knockdown shows that EML3 has an important role in correct alignment of chromosomes in metaphase. Our analysis therefore identifies EML3 as an interesting human gene product involved in correct spindle function and validates our identification and characterisation strategy for novel proteins required for correct cell division.

Results

To specifically purify microtubule-binding proteins from nuclei we first prepared a soluble fraction of nuclear proteins free from cytoplasmic tubulin (nuclear extract, NE). We lysed cells with digitonin in the presence of nocodazole and isolated nuclei by centrifugation. Nuclei were then extracted at high ionic strength and nuclear remnants removed by centrifugation (Fig. 1A). Proteins in the resulting extracts were analysed by immunoblot using antibodies against different marker proteins (Fig. 1B). Human TPX2, which locates to the nucleoplasm during interphase and to the spindle in mitosis (Heidebrecht et al., 1996; Gruss et al., 2002), was only seen in the nuclear fraction. By contrast, tubulin, actin and the cytoplasmic MAP OP18/Stathmin (Curmi et al., 1999) were almost exclusively, and Hsc70 mainly, found in the cytosolic fraction (Fig. 1B). The majority of RCC1, a chromatin-associated nuclear protein (Bischoff et al., 1990) was found in nuclear extracts (Fig. 1B).

Next, we re-added microtubules to NE and purified them by sedimentation (Fig. 1A,C, lower panel). Under these conditions, RCC1, which is a marker for non-microtubule-associated nuclear proteins, remained in the supernatant (Fig. 1C, middle panel, lanes

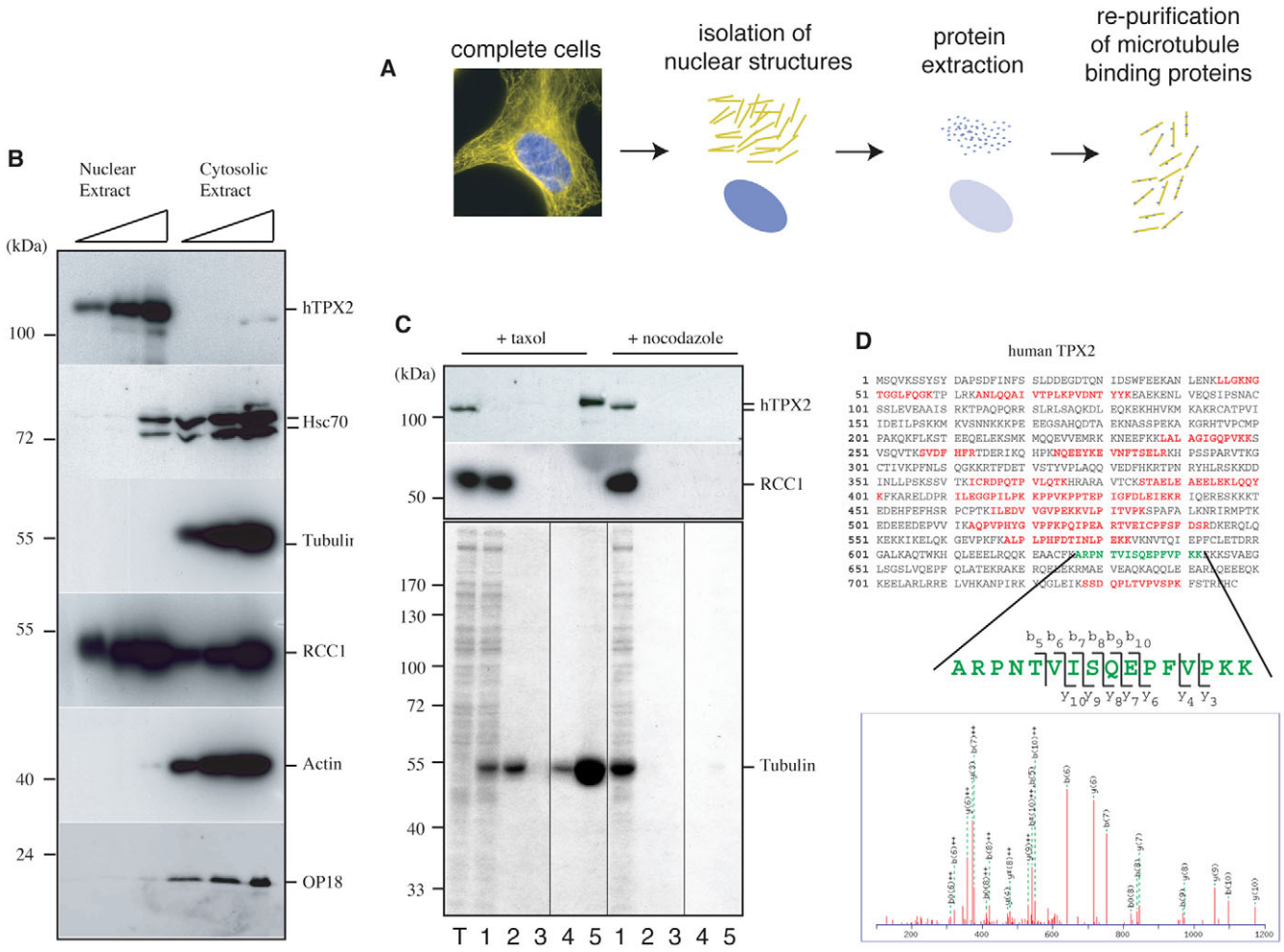

Fig. 1. Purification of microtubule-binding proteins from nuclear extracts. Purification scheme (A) and analysis of nuclear extracts (nu) or cytosolic extracts (cyt) by immunoblot (B) using specific antibodies to the human nuclear MAP TPX2 (hTPX2), the cytosolic chaperone Hsc70, α-tubulin, the chromatin protein RCC1, β-actin or the cytoplasmic MAP OP18/Stathmin. (C) Analysis of MAP purification by sedimentation in the presence of taxol or nocodazole. Nuclear extract (T), supernatant (1) or pellet (2) after first microtubule spindown and supernatant (3) or pellet (4 and 5, 10× amount) after second microtubule spindown were analysed by silver staining of total protein (lower panel) and immunoblot using antibodies specific to RCC1 (middle panel) or and human TPX2 (hTPX2, upper panel). Expected running behaviour on SDS gels (B and C, right) and respective molecular weights (B and C, left) are indicated. Note that probably owing to posttranslational modification (see gel retardation in the SDS gel), TPX2 in the microtubule pellet fraction (Fig. 1C, lane 2) was consistently more difficult to detect by immunoblotting than in total (T) or the supernatant (1) and only visible after long exposure times. (D) Protein sequence of human TPX2 (upper panel) and representative ion spectrum (lower panel). Identified peptides are shown in red and green, respectively, which resulted in a sequence coverage of 30%. The fragment ion spectrum of the peptide coloured in green is shown in the lower panel. C-terminal fragment ions of the peptide are labelled as y fragments, N-terminal fragments as b. The numbers of their respective N-terminal amino acid (y) or C-terminal amino acid (b) are indicated. Doubly charged fragments are labelled (++), all other fragments were singly charged.

T and 1). By contrast, we detected TPX2 in the microtubule pellet fraction (Fig. 1C, upper panel). Although immunoblot detection of TPX2 was more difficult in microtubule pellet fractions than in total extracts and supernatants (see Fig. 1C, lanes T, 1, 2 and 5), we estimated a recovery of at least 10% of TPX2 in the final microtubule sediment using quantitative immunoblot analysis (Fig. 1C and data not shown). No proteins were visible in the pellet fraction when taxol was replaced with nocodazole to prevent microtubule polymerisation (Fig. 1C, compare lanes 5 in taxol and nocodazole samples). For the proteomic survey of nuclear MAPs, we separated proteins of the microtubule pellet fraction on a preparative SDS gel and identified proteins by tandem mass spectrometry (see methods for details). TPX2, the positive control, was identified on the basis of 13 nonoverlapping peptides covering 30% of its sequence (Fig. 1D). Initially, after LC-MS/MS analysis and filtering redundant sequences we identified 374 unique human protein sequences. Of these, 324 had assigned functions and 50 were poorly or not at all characterised (supplementary material Table S1).

Interestingly, we also found 10 subunits of the anaphase-promoting complex (APC) with high sequence coverage (22-49%). Topper et al. have previously shown that APC3 localises to spindle microtubules and spindle poles (Topper et al., 2002) and APC3, APC6 and the phosphorylated form of APC1 were also seen to localise to kinetochores in prophase immediately before nuclear envelope breakdown (Acquaviva et al., 2004; Kraft et al., 2003). To determine localisation of the APC in intact cells, both in interphase and M phase, we visualised different APC subunits using specific antibodies (supplementary material Fig. S1). Indirect immunofluorescence using these antibodies revealed nuclear accumulation of all APC subunits; in addition, APC7 could be detected on cytoplasmic microtubules in interphase. Moreover, our data show spindle localisation of APC3, APC5 and APC7 in M phase (supplementary material Fig. S1). These observations confirm nuclear as well as spindle localisation of proteins identified here and therefore validate our purification scheme. These data also suggest that several APC subunits form a complex in the interphase nucleus and relocalise to the spindle in M phase.

We then went on to analyse the poorly characterised open reading frames (ORFs). We generated cDNA constructs for EYFP fusion proteins of poorly characterised ORFs from available ESTs (supplementary material Table S2) and transfected them into human HeLa cells to analyse the localisation of the expressed fusion proteins in interphase and mitosis. When we determined the localisation of 18 human ORFs, which at the time of our analysis were poorly characterised, we found five proteins showing strong accumulation at the spindle (Fig. 2 and supplementary material Table S2) and another three enriched at the site of the spindle (supplementary material Table S2).

One of the proteins identified in our screen and validated by localisation of its YFP fusion was the translation product of the FLJ46843 cDNA (supplementary material Tables S1 and S2). Its sequence showed that this protein belongs to the family of human echinoderm microtubule associated proteins (EMAPs). The expression product of FLJ46843 is also referred to as human EML3. All the EMAP proteins have a name-giving conserved motif in common (hydrophobic EMAP-like protein domain, known by the acronym HELP), which is thought to mediate direct microtubule binding. EMAP-like proteins from different species have been shown to bind to microtubules in interphase and mitosis (Suprenant et al., 2000).

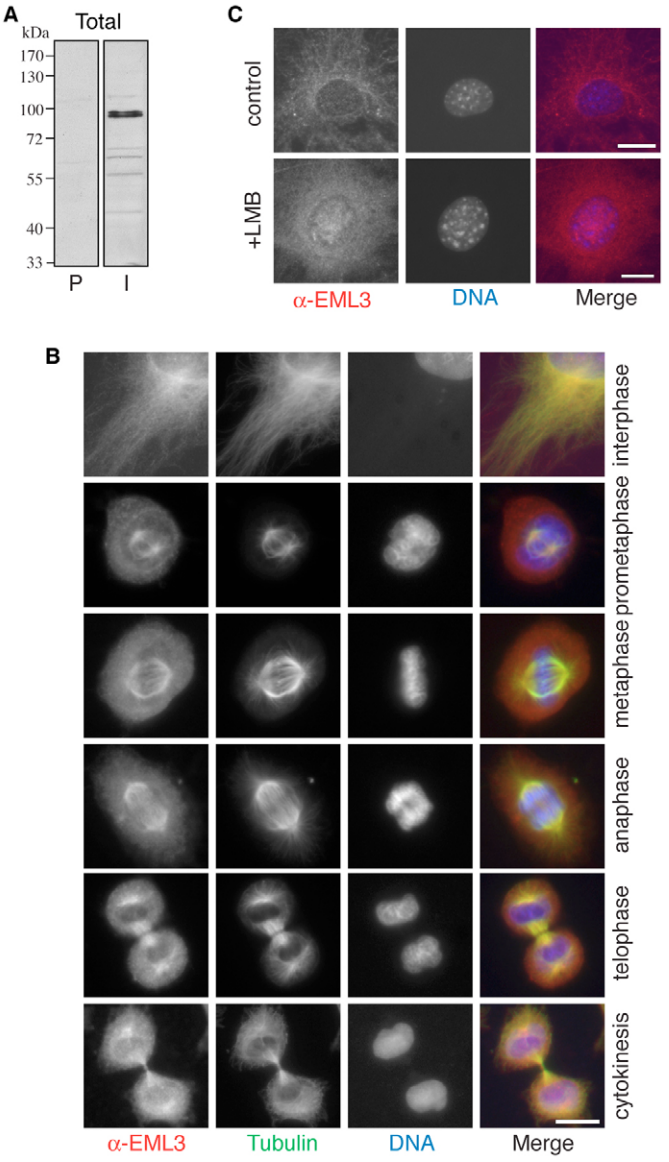

Fig. 2. Characterisation of EML3 localisation by indirect immunofluorescence. Antibodies against human EML3 peptide sequences were used to detect the protein by immunoblot or immunofluorescence. (A) Immunoblots of total lysates of HeLa cells. P, preimmune serum; I, EML3 immune serum. (B) Localisation of EML3 in the different mitotic phases and in interphase of HeLa cells as indicated. Cells were fixed with methanol at –20°C and stained with serum against EML3 (middle left panels and red colour in merge), α-tubulin (middle right panels and green colour in merge) and with DAPI to visualise DNA (blue colour in merge). (C) EML3 was detected by indirect immunofluorescence after fixation with formaldehyde in interphase HeLa cells before and after addition of leptomycin B (LMB) to inhibit CRM1-dependent nuclear export. Scale bars: 10 μm.

To examine the subcellular localisation of endogenous human EML3, we generated antibodies using two specific peptides within the human EML3 sequence as antigens. Consistent with the predicted molecular weight of the human EML3/EMAP95, these antibodies recognised a signal at the molecular weight of 95 kDa in immunblots on total HeLa cell lysates. This signal was not shown by preimmune sera, confirming the specificity of our antibodies (Fig. 2A, left panel). Indirect immunofluorescence after fixation of cells with methanol using these antibodies demonstrated the

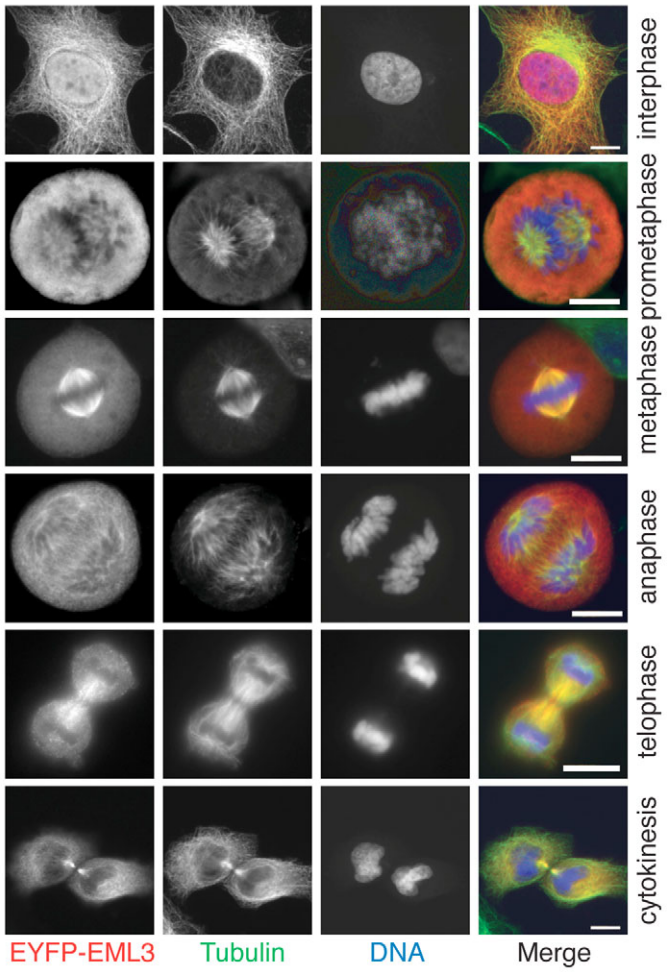

Fig. 3. Characterisation of YFP-EML3 localisation. Images show the localisation of the EYFP-EML3 fusion protein in interphase and in the different mitotic phases as indicated. Cells were fixed with methanol at –20°C and stained with antibodies against GFP (middle left panels and red colour in merge), α-tubulin (middle right panels and green colour in merge) and with DAPI to visualise DNA (blue colour in merge). Scale bars: 10 μm.

localisation of human EML3 on microtubules throughout all mitotic stages (Fig. 2B). EML3 localised all along microtubules without a preference for one end of the polymers or one particular population of spindle microtubules. EML3 was clearly detectable from prometaphase on and remained on microtubules even during cytokinesis, where it localised to the midbody (Fig. 2B, cytokinesis). EML3 also colocalised with microtubules in interphase (Fig. 2B, interphase). To analyse whether EML3 was also present in interphase nuclei, we fixed cells with formaldehyde and determined the localisation of EML3 by indirect immunofluorescence before and after inhibition of CRM1-mediated protein export by leptomycin B (Fig. 2C). We readily detected an increase in the nuclear signal of EML3 upon leptomycin B treatment, suggesting a nuclear pool of EML3 in HeLa cells in interphase (Fig. 2C). Consistent with this, EML3 was found in both the cytosolic and nuclear fraction of HeLa lysates (data not shown). Taken together, these data show that EML3 is a microtubule-binding protein throughout all cell cycle stages and suggest that the protein shuttles between the cytoplasm and nucleus during interphase.

To determine which motifs in human EML3 mediate microtubule binding and nuclear localisation, respectively, we analysed the subcellular localisation of human EML3-YFP fusion proteins (Fig. 3). Expression of YFP-tagged full-length human EML3 in HeLa cells indicated colocalisation with cytoplasmic microtubules (Fig. 3), and, consistently with our immunofluorescence data, we observed accumulation of EML3 in interphase nuclei (Fig. 3). By contrast, expression of the closely related human EML2 did not reveal nuclear accumulation (data not shown). When we determined the localisation of YFP-EML3, we again observed colocalisation with microtubules throughout all mitotic stages (Fig. 3). The accumulation of YFP-EML3 on spindles in metaphase was rapidly lost upon incubation of cells with nocodazole (data not shown), confirming microtubule-dependent localisation of EML3. Consistently with the localisation of endogenous human EML3, we could also detect YFP-EML3 on spindle microtubules in anaphase and on the midbody during cytokinesis, when nuclei had already reassembled (Fig. 3, cytokinesis).

When we analysed the primary structure of EML3, we spotted a short stretch of basic amino acids in the C-terminal proximity of the HELP domain, which was predicted to be a nuclear localisation signal (NLS, Fig. 4). Indeed, a mutant version of EML3, in which two of the five basic amino acids within the potential NLS had been replaced by alanines, did not show nuclear accumulation in interphase. Colocalisation with microtubules in interphase and metaphase was, however, still observed (Fig. 4, ΔNLS).

In order to verify the function of the HELP domain of EML3 in microtubule binding, we generated a fragment of EML3, in which the first 168 N-terminal amino acids, including the HELP domain but not the putative NLS, were deleted (EML3ΔN). EYFP-EML3ΔN still accumulated in the nucleus but did not show detectable colocalisation with microtubules (Fig. 4). In turn, EYFP fused to the N-terminal 168 amino acids (EML3N) did show colocalisation with microtubules in interphase although this was weaker than the full-length protein (Fig. 4). However, no accumulation of this fusion protein on the spindle could be observed in mitosis (Fig. 4). Taken together, this indicates that the HELP domain is required for microtubule colocalisation and might suggest that this motif is sufficient to mediate microtubule binding of EML3 in interphase. It also shows that a subpopulation of EML3 is sequestered in the nucleus.

The prominent localisation of human EML3 on mitotic microtubules suggested a function of EML3 in spindle formation or chromosome segregation. We therefore investigated a potential mitotic function of EML3 using RNA interference (RNAi)-mediated mRNA knockdown. We transfected cells with two different siRNA oligonucleotides to knockdown EML3 and determined relative mRNA levels by quantitative RT-PCR compared with scrambled nontargeting siRNAs as controls (Fig. 5A, left panel). The mRNA knockdown was efficient for both oligos 24 hours after transfection. Immunoblot analysis using specific antibodies against human EML3 (see Fig. 2) verified the knockdown of endogenous EML3 with residual levels of approx. 15-35% 72 hours after transfection with siRNA oligos (Fig. 5A, right panel).

Next, we used time-lapse imaging to detect potential phenotypes observed after reduction of EML3 independently of the time of their occurrence. siRNA duplexes and transfection reagent were spotted and dried on regular grids on chambered LabTek coverglasses and HeLa Kyoto cells were plated on the siRNA microarrays (time 0). Under these conditions, 99% of all cells are transfected with siRNA oligos (Neumann et al., 2006). To directly monitor nuclear division

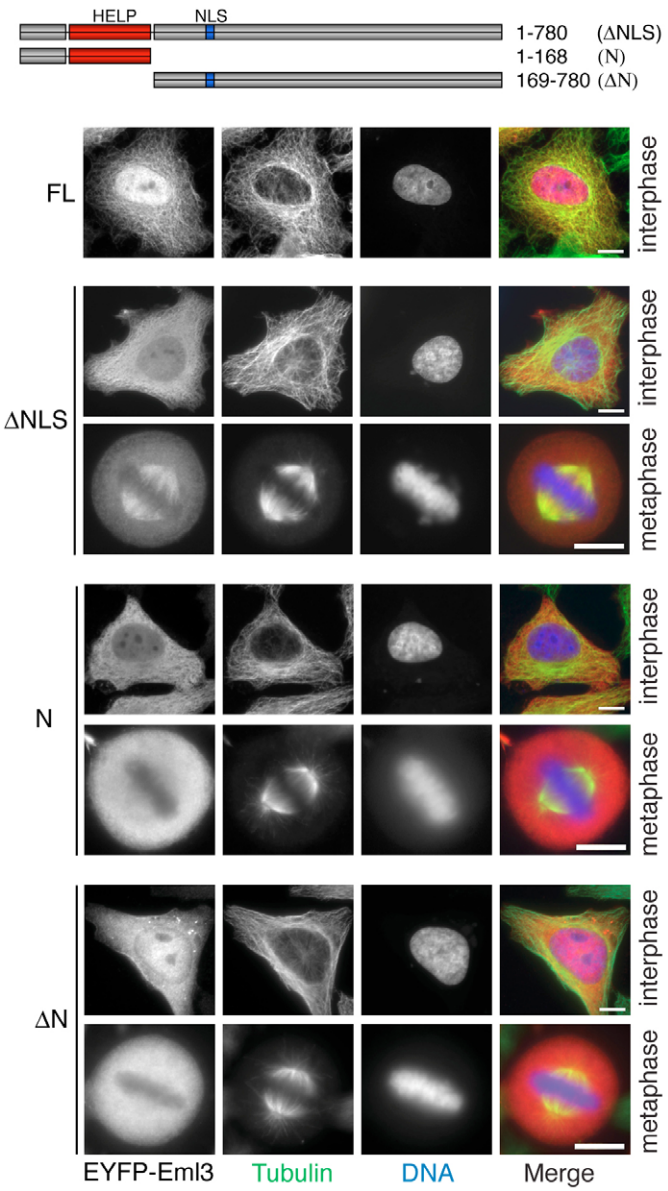

Fig. 4. Domain analysis of Eml3. Schematic representation is shown at the top of the constructs used to prepare images below. From the full-length (FL) human EML3 (see also Fig. 2), two basic amino acids were replaced to corrupt the nuclear localisation signal (ΔNLS). An N-terminal fragment (amino acids 1-168, N) contained the HELP domain, whereas the N-terminal 168 amino acids including the HELP domain were missing in the ΔN construct. The EYFP-Eml3 fusion constructs (EYFP-Eml3) were visualised in interphase or metaphase, respectively. Cells were fixed with methanol at –20°C and stained with antibodies against GFP (middle left panels and red colour in merge), α-tubulin (middle right panels and green colour in merge) and with DAPI to visualise DNA (blue colour in merge). Scale bars: 10 μm.

with time, we used cells stably expressing EGFP-Histone 2B. We recorded the EGFP signal 29 hours after seeding the cells for an additional 48 hours using time-lapse microscopy over 30-minute frame intervals. Automatic data analysis scored the overall proliferation rate and the three biological classes: apoptosis (apoptotic index); mitosis (mitotic index); and irregular nuclear shape [shape index (Neumann et al., 2006)]. We now determined these indices over time (blue lines in Fig. 5B) in EML3 knockdown and control siRNA-treated cells (control mean ± s.d. of four experiments; grey band in Fig. 5B) on the same siRNA microarray. After treatment with oligos against the *Eml3* gene product, cells scored in all categories, showing an increase in the mitotic index (2/2 oligos), the shape index (2/2 oligos) and the apoptotic index (2/2 oligos) (Fig. 5B). Treatment with either oligo also led to a reduction of the overall proliferation rate (Fig. 5B, proliferation, 2/2 oligos).

To document the delay in mitosis with higher temporal resolution, we imaged cells in which EML3 had been knocked-down, every 5 minutes and compared them to control cells (Fig. 5C, supplementary material Movie 1). In control cells, correctly aligned chromosomes were regularly visible in 3-4 consecutive frames (i.e. for 15-20 minutes) before chromosome segregation started (Fig. 5, control siRNA). By contrast, EML3 knockdown caused cells to delay in metaphase for several hours, chromosomes were apparently less well aligning and cells often underwent apoptosis (Fig. 5C, EML3 RNAi and supplementary material Movie 2).

To analyse the suggested mitotic phenotype of EML3 knockdown in more detail, we determined the mitotic index by counting a large number of cells 80 hours after inverse transfection with siRNA oligonucleotides specific for *Eml3* (Fig. 6). We observed an increase in the overall mitotic index after EML3 knockdown as judged by the number of cells with condensed chromosomes (Fig. 6A, left panel), which was largely explained by an elevated number of cells found with metaphase-like structures (Fig. 6A, right panel).

Accumulation of cells in metaphase argues for the activation of the spindle assembly checkpoint, which blocks progression of cells into anaphase until all chromosomes are bivalently attached to spindle microtubules and aligned in the metaphase plate. This could mean that knockdown of EML3 causes inefficient bipolar microtubule attachment and delays alignment of chromosomes in metaphase. To test this hypothesis, we visualised microtubules and chromatin in mitotic cells after EML3 knockdown or in control cells, respectively. Although the efficiency of assembling spindles with normal spindle bipolarity (i.e. the appearance of two focused poles) was not changed (Fig. 6B, quantification), after knockdown of EML3, cells showed a 20-fold (±1.51, oligo 1) or 24-fold (±1.26, oligo 2) higher frequency of spindles with unaligned chromosomes or chromosomes spreading out from the metaphase plate (Fig. 6B). To gain to another quantitative result for the apparent defects in chromosome alignment, we measured the extension of chromatin along the pole-to-pole axis in control or EML3-knockdown cells. Indeed, we observed a highly significant ($P<10^{-10}$) increase in the average chromatin extension values changing from 2.5±0.18 μm in controls, to 5.0±0.65 μm (oligo 1) or 5.3±1.33 μm (oligo 2) after EML3 knockdown (Fig. 6C). The increase in chromosome extension was accompanied by elevated relative variations of the measured values (Fig. 6C, right bars in quantification and blue and red rectangles in plot).

In summary, these data show that EML3 is required for correct spindle function and chromosome capture in metaphase, and represents a valid example that proteins identified in our screen are promising candidates as novel factors required for correct cell division.

Discussion

Open mitosis in higher eukaryotes enables the recruitment of many proteins from the nuclear compartment to the spindle apparatus. Here we have focused on the identification of novel proteins of this category. We started with a proteomic survey of proteins co-purifying with microtubules from nuclear extracts to generate a list of candidates.

Of the 374 proteins found in our analysis, 42% were also identified in the proteomic survey of human spindles (Sauer et al., 2005). Among the most abundant microtubule-binding proteins identified in our screen were 10 subunits of the APC, all of which we identified with high and comparable peptide coverage. Analysis of their localisation by indirect immunofluorescence validated the specificity of our method and suggested that the APC is indeed nuclear during interphase and localises to the spindle in mitosis, as suggested previously (Kraft et al., 2006; Topper et al., 2002; Acquaviva et al., 2004; Kraft et al., 2003; Gieffers et al., 1999).

Our screen revealed 50 human open reading frames, which at the start of our investigations had been only poorly, or not at all, characterised. Eighteen of them were analysed using expression of corresponding EYFP fusion proteins; five showed strong spindle accumulation (EML3, Kif16B, MAP1S, SPATA5 and C20ORF129, supplementary material Table S2) and three further proteins were enriched at the site of the spindle (SPATA5-like, MGC2714, P30 DBC protein). Three of these gene products have now been published as microtubule-binding or spindle proteins [MAP1S (Orban-Nemeth et al., 2005; Dallol et al., 2007), Kif16B (Hoepfner et al., 2005) and C20ORF129 (Sauer et al., 2005)]. The function of C20ORF129 is still elusive, whereas a role for Kif16B in the transport of early endosomes to microtubule plus ends in the cell periphery has been established (Hoepfner et al., 2005). One interesting hypothesis is that Kif16B has the same primary function in interphase as well as in mitosis and might segregate vesiculated membrane organelles along spindle microtubules to the arising daughter cells in M phase. We also identified two uncharacterised ATPases associated with various cellular activities (AAA-ATPases), SPATA and SPATA5-like as spindle proteins and are currently testing potential mitotic functions of these gene products.

Out of our initial list of candidates, we further focused on the functional analysis of human EML3, a poorly characterised member of the EMAP family. Other EMAPs have been shown to be microtubule-binding proteins in interphase and M phase in sea urchins (Suprenant et al., 1993) and, more recently, also in human cells (Suprenant et al., 2000; Pollmann et al., 2006). Our indirect immunofluorescence shows that the protein is microtubule associated throughout all stages of mitosis, as well as in interphase. All EMAP proteins share a common HELP domain, a hydrophobic motif which is supposed to be responsible for direct microtubule-binding as previously shown for the closet EML3 orthologue EML4/Ropp120 (Pollmann et al., 2006). We confirmed this assumption using a truncated version of EML3, in which the HELP domain was missing. This truncated version of EML3 did not colocalise with microtubules, either in interphase or in mitosis. In turn, the N-terminal fragment including the HELP domain still colocalised with microtubules in interphase. However, this protein fragment did not accumulate on mitotic spindles. This might mean that the HELP domain is not sufficient to mediate microtubule binding in mitosis and that the C-terminal part of the protein contributes to the regulation of microtubule binding in mitosis. Phosphorylation mediated by CDC2 (also known

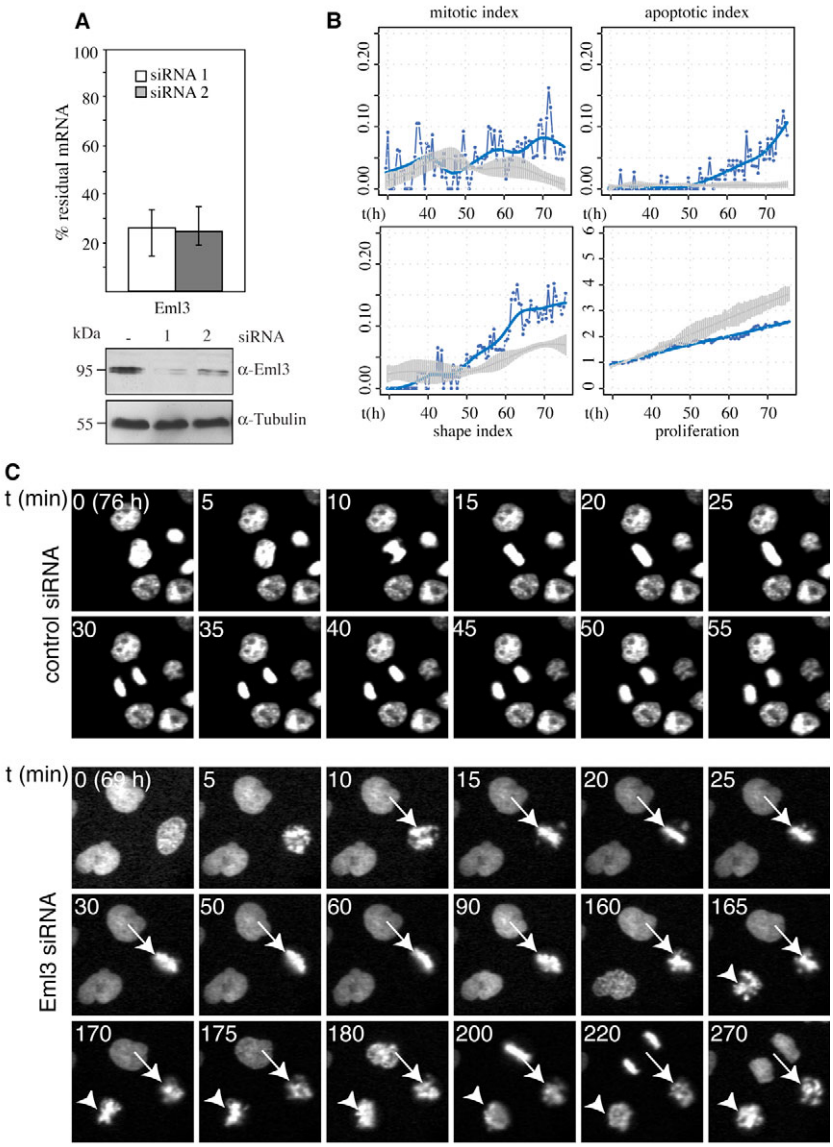

Fig. 5. Phenotypic analysis of EML3 knockdown using time-lapse imaging. (A) siRNA oligos specific for *Eml3* (80 nM) were used to knockdown the respective mRNAs in HeLa Kyoto cells; the same concentration of scrambled, nontargeting siRNAs served as a control. Left panel, qRT-PCR quantification of siRNA-mediated gene knockdown 24 hours post transfection (see experimental procedures). The relative remaining levels of target mRNA expression normalised by *GAPDH* mRNA was measured compared with cells transfected with scrambled siRNA oligos. Error bars represent the maximum and minimum expression levels of three individual experiments. Right panel, total cell lysate was prepared from HeLa cells before and after knockdown of EML3 using two different siRNA oligonucleotides (1 and 2) and EML3 was detected by immunoblot using specific antibodies. Tubulin served as a loading control. (B) siRNA oligos were used to knockdown EML3 in HeLa Kyoto cells stably expressing Histone 2B-EGFP. 29 hours after transfection, the EGFP signal was recorded at intervals of 30 minutes for another 48 hours. Automatically analysed phenotypes were classified and indices of mitosis, apoptosis, shape and the overall proliferation rate plotted over time. Results of representative experiments are plotted in blue (continuous line, fitted curve; dotted line, measured data points) and the control confidence band (mean ± s.d.) in grey. (C) The EGFP signal was recorded for 14 hours at intervals of 5 minutes, 60 hours after siRNA oligo transfection. Sections from selected frames were used for still images, times after seeding (i.e. transfection of) the cells (in brackets) and time intervals from the respective starting points are indicated.

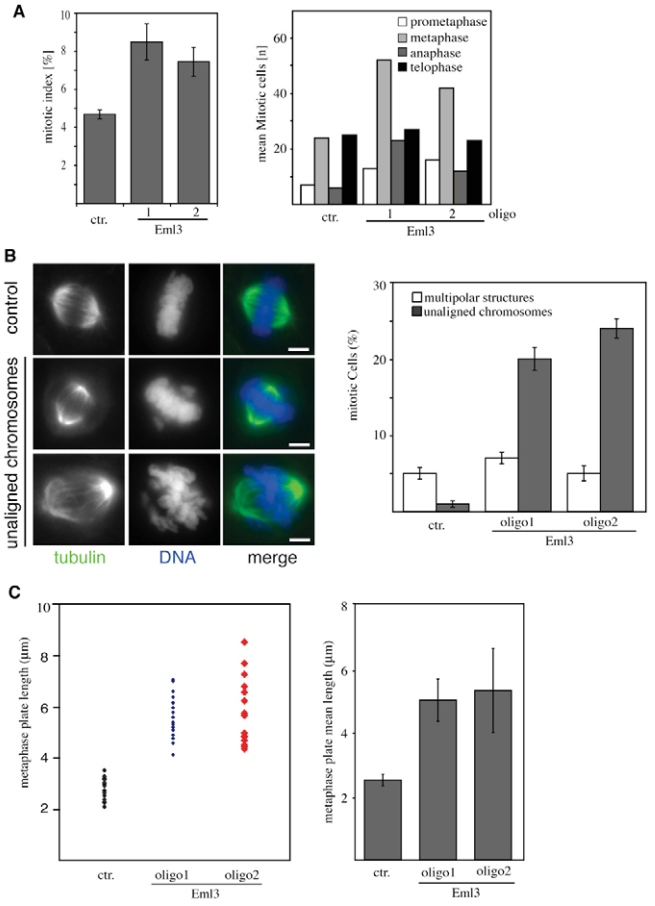

Fig. 6. Analysis of EML3 function in spindle formation. Knockdown of EML3 was performed as described in Fig. 5 using two different siRNA oligonucleotides specific to EML3 (1 and 2) and cells fixed with paraformaldehyde 80 hours post transfection. (A) Mitotic indices after gene knockdown were determined from 480 cells and means and s.d. from three independent experiments were plotted (left panel). The sums of cells at the different mitotic stages after gene knockdown were determined in the mitotic cells (right panel). (B) Representative immunofluorescence images of aberrant metaphase-like structures with unaligned chromosomes. Merge: DNA (blue) and Tubulin (green). Scale bars: 10 µm. Quantification of phenotypes resulting from EML3 knockdown is shown on the right. Means ± s.d. from three independent experiments (n=100) were plotted. (C) The maximum extension of metaphase chromosomes in a virtual pole-to-pole axis of the mitotic spindle was determined in 20 images after treatment with the respective siRNA oligos as indicated. Single values (left) and average values and s.d. (right) were plotted.

as CDK1), of which several consensus sites are predicted in the C-terminus of EML3, could, for example, mediate this regulation.

Alternatively, the subcellular localisation of EML3 might regulate the overall activity of the protein towards microtubules. Indirect immunofluorescence to determine the localisation of endogenous EML3 and analysis of the distribution of overexpressed YFP-EML3 suggest that EML3 shuttles between the cytoplasm and nucleus. However, although the level of endogenous EML3 in the nucleus was low in the absence of leptomycin B, the YFP fusion readily accumulated. It is possible that GFP tagging or overexpression caused a change in the equlibrium between import and export rates of YFP-EML3. Supporting the idea that EML3 is actively imported into the nucleus, we identified an NLS responsible for nuclear accumulation of YFP-EML3. It might therefore be speculated that a proportion of EML3 is sequestered in the nucleus to reduce its levels in the cytoplasm. Entry into mitosis and nuclear envelope breakdown would then allow additional EML3 to be recruited to microtubules. It is also possible that the nuclear population of EML3 could be separately modified, for example, in preparation for mitosis-specific functions. Nuclear accumulation of EML3 and the identification of a functional basic NLS also strongly suggests interaction of the protein with the nuclear transport receptors importin-α and -β and raises the possibility that EML3 is regulated by importins and the Ran system in mitosis. Similarly, the recently identified spindle protein hepatoma-upregulated protein (HURP) can shuttle between the cytoplasmic and the nuclear compartment and is also regulated by importin-β and the Ran system (Sillje et al., 2006).

To determine the importance of EML3 in spindle function in mitosis, we used siRNA-mediated knockdown of EML3. Treatment with siRNA oligonucleotides specific for *Eml3* efficiently reduced EML3 protein levels but a 15-35% residual amount remained. Studies in the sea urchin model system suggest that EMAPs are among the most abundant microtubule-binding proteins (Suprenant et al., 2000) and it is likely that a complete knockdown will be difficult to realise. Nevertheless, knockdown of EML3 under these conditions led to an increase in the mitotic index of human cells consistent with an important function of the protein in mitosis in human cells. Cells treated with siRNA oligonucleotides specific for *Eml3* often remained in a metaphase-like state for several hours. Detailed analysis revealed aberrant metaphase-like structures, displaying unaligned chromosomes or few chromosomes still spreading out from the metaphase plate. Recent data on EML4/Ropp120 suggest that this protein is required for microtubule organisation (Pollmann et al., 2006) and that its overexpression stabilises interphasic microtubules in intact cells (Houtman et al., 2007). By contrast, the human EMAP-like protein 70 (Elp70 or EML2) mediated microtubule destabilisation when tested in vitro. Based on this activity, EML2 was proposed to add to the reorganisation of microtubules in M phase, when a general decrease in microtubule stability is observed (Eichenmuller et al., 2002). It might be speculated that EML3 functions to destabilise microtubules evenly and contributes to the increase in catastrophe rate in early mitosis, which enables highly dynamic mitotic microtubules. Although we do not know the precise mode of action of EML3 on mitotic microtubules, our data clearly indicate that loss of EML3 function causes problems in 'search and capture'. This delays bivalent attachment of chromosomes to microtubules and activation of the spindle assembly checkpoint.

In summary, we describe an approach to identify novel spindle proteins using a combination of proteomics, localisation analysis and an automated, very sensitive assay for cell division and proliferation. The detailed functional validation of one of the identified proteins, EML3, demonstrates that this combination of methods provides an ideal platform, not only to identify proteins involved in cell division but also to characterise them.

Materials and Methods

SDS page and immunoblotting

Analytical and preparative SDS PAGE was performed as described (Laemmli, 1970).

Antibodies and reagents

Antibodies against human EML3 were generated in the guinea pig against a mix of two peptides: 165-175 (RPRQKLSRKAI and an additional C for coupling to KLH) and 759-775 (CKQLKNRYESRDREWAT) of Q32P44, Q6ZQW7, Q8NA55 Swiss Prot ID coupled to KLH. KLH-coupled peptides were also used for preincubation with the antigenes. The following antibodies were used for immunofluorescence and immunoblot: rabbit polyclonal anti-GFP (a gift from Dirk Görlich, MPI für Biophysik, Göttingen, Germany), anti-α-tubulin (Sigma, monoclonal mouse, T9026), anti β-actin (Sigma, monoclonal mouse, A5441), anti-TPX2 [rabbit polyclonal (Gruss et al., 2002)]

and anti-RCC1 [rabbit polyclonal (Hetzer et al., 2000)]. Anti-Hsc70 (rabbit polyclonal) was a gift from Bernd Bukau (ZMBH, Heidelburg, Germany), anti-OP18 (rabbit polyclonal) was a gift from Tony Hyman (MPI für Molekulare Zellbiologie und Genetik, Dresden, Germany). APC4 and APC7 antibodies were gifts from Franz Herzog and Jan-Michael Peters (IMP, Vienna, Austria). APC5 antibody (rabbit polyclonal) was purchased from Abcam (ab4170). APC3 antibodies were generated in rabbit using a conserved peptide of the protein as described (Dube et al., 2005). Leptomycin B (used at 10 ng/ml for 60 minutes) was purchased from LC labs (Woburn, MA).

Preparation of nuclear extracts (NE)

A cell mass corresponding to 5×10^9 cells [HeLa whole cell pellet from Cilbiotech (Mons, Belgium)] was used for nuclear extract preparation. Cells were washed with PBS, resuspended in nocodazole-containing lysis buffer [20 mM HEPES, pH 7.6, 100 mM KCl, 1 mM $MgCl_2$, 8.6% glycerol, 1 mM DTT, 5 μM nocodazole (Sigma), 5 μM cytochalasin B (Sigma), 0.2% digitonin (complete protease inhibitor mix (Roche)] homogenised in a Dounce homogeniser and layered on top of a 25 ml cushion/6×10^8 cells (cushion solution: lysis buffer without nocodazole, without digitonin, 30% glycerol). Nuclei were centrifuged at 800 ***g*** for 10 minutes at 4°C, washed in wash buffer (cushion solution with 8.6% glycerol) and recentrifuged. The nuclear pellet was resuspended in two volumes of extraction buffer (10 mM HEPES pH 7.6, 500 mM KCl, 1 mM $MgCl_2$, 25% glycerol, 1 mM DTT, 5 μM cytochalasin and protease inhibitors), homogenised and stirred for 30 minutes. Nuclear extracts were obtained by centrifugation at 25,000 ***g*** for 30 minutes and dialysing the resulting supernatant twice for 2 hours each against 100 volumes of dialysis buffer (10 mM HEPES pH 7.6, 100 mM KCl, 1 mM $MgCl_2$, 20% glycerol, 1 mM DTT). To avoid protein sedimentation in the absence of microtubules, the dialysed crude NE was centrifuged again for 60 minutes at 250,000 ***g*** in a TLA120.2 (Beckman) rotor. Protein concentration of resulting final nuclear extracts (NE) was usually 2.5 mg/ml and we obtained ~15 ml from 5×10^9 cells.

MAP isolation

Polymerised microtubules from porcine brain tubulin (corresponding to initial concentration of 230 μM tubulin in BRB80) (Mitchison and Kirschner, 1984) were added to a final concentration corresponding to 6.7 μM tubulin to 1.5 ml NE in the presence of 1 mM GTP, 1 mM AMP-PNP, 150 mM KCl, 1 mM $MgCl_2$, 10 μM cytochalasin B and 10 μM Taxol and further incubated for 30 minutes at 30°C. The reaction was layered on top of 2 ml cushion solution (10 mM HEPES, pH 7.6, 150 mM KCl, 1 mM GTP, 1 mM AMP-PNP, 1 mM $MgCl_2$, 1 mM DTT, 30% glycerol, 10 μM cytochalasin B and 10 μM Taxol), centrifugation for 10 minutes at 37,000 ***g*** in a TLA100.3 rotor (Beckman). The resulting microtubule pellet was resuspended in 0.33 volumes repolymerisation buffer (10 mM HEPES, pH 7.6, 20% glycerol, 1 mM GTP, 1 mM AMP-PNP, 150 mM KCl, 1 mM $MgCl_2$, 10 μM cytochalasin B and 10 μM Taxol), and recentrifuged as described above. The final microtubule pellet was resuspended in SDS sample buffer (Laemmli, 1970) after denaturing for 10 minutes at 65°C was centrifuged for 10 minutes at 250,000 ***g*** in a TLA100.2 rotor (Beckman) to remove tubulin aggregates that otherwise interfered with separation of the sample. The supernatant was loaded on a 1.5-mm-thick preparative 10% SDS gel (Laemmli, 1970).

Identification of proteins in the microtubule pellet fraction

We systematically identified proteins from the tubulin-containing lane of the preparative SDS gel. The gel was therefore cut into 32 gel slices and all slices digested in gel with trypsin. The resulting tryptic peptides were separated by reversed-phase nano HPLC and analysed with ESI quadrupole time-of-flight mass spectrometry. Peak-lists from MS/MS spectra were searched against the human IPI database using the Mascot software. Since the IPI protein database contains sequences that are not distinguishable using mass spectrometers, we removed redundancy.

In-gel tryptic digestion and LC-MS/MS analysis

Proteins of the final microtubule fraction were separated on a preparative 10% SDS gel. Proteins present in the gel lane were visualised with colloidal Coomassie Blue staining. Readily visible bands were excised with a scalpel. The remaining gel lane was then cut into equal-sized pieces of approximately 3 mm each. Gel slices were transferred to a 96-well plate and reduced, alkylated and digested with trypsin (Catrein et al., 2005) using a Digest pro MS liquid handling system (Intavis). Following digestion, tryptic peptides were extracted from the gel pieces with 50% acetonitrile/0.1% trifluoroacetic acid (TFA) concentrated nearly to dryness in a speedVac vacuum centrifuge and diluted to a total volume of 30 μl with 0.1% TFA. 25 μl of each sample was analysed by a nano HPLC system (Ultimate, Dionex, equipped with a Famos autosampler) coupled to an ESI quadrupole time-of-flight mass spectrometer (QSTAR pulsar; Applied Biosystems). Samples were loaded on an Inertsil C18 trapping column (GL Sciences) with a flow rate of 20 μl/minute 0.1% TFA. Peptides were eluted and separated on an analytical column (75 μm × 150 mm) packed with Inertsil 3 μm C18 material with a flow rate of 200 nl/minute in a gradient of buffer A (0.1% formic acid/5% acetonitrile) and buffer B (0.1% formic acid, 80% acetonitrile): 0-2 minutes: 5% B; 2-50 minutes: 5-40% B; 50-60 minutes: 40-60% B; 60-63 minutes: 60-90% B. The column was connected to a nano ESI emitter (New Objective). 2000 V were applied via liquid junction. The quadrupole time-of-flight mass spectrometer (QSTAR pulsar; Applied Biosystems) operated in positive ion mode. One MS survey scan (0.7 seconds) was followed by one information dependent product ion scan (3 seconds). Only doubly and triply charged ions were selected for fragmentation.

Identification of MS/MS spectra by database searches

From the MS/MS spectra, peak lists were generated without peak removal after centroiding and deisotoping (analyst QS 1.1; Applied Biosystems; combined with Mascot script version 1.6b13; Matrix Science). The peak list was then applied to a database search against the IPI human database (57,478 entries; downloaded 6 September 2005) using the Mascot software version 2.1 (Matrix Science). The algorithm was set to use trypsin as the enzyme, allowing a maximum of one missed cleavage site and assuming carbamidomethyl as a fixed modification of cysteine, and oxidised methionine and deamidation of asparagines and glutamine as variable modifications. Mass tolerance was set to 1.1 Da and 0.1 Da for MS and MS/MS, respectively. A protein hit was required to include at least one bold red peptide match to get the minimum list of proteins sufficient to explain all observed peptides. The maximum number of hits was set to auto, which displays all proteins containing at least one peptide with an ion score exceeding the significance threshold ($P<0.05$). Data of each gel slice were searched separately. For proteins detected in several gel slices, only the highest scoring value of a single analysis is given. Proteins identified by a single peptide are listed in the tables only after manual evaluation of the fragment spectrum following similar criteria as suggested (Chen et al., 2005): (1) The peptide ion score, based on absolute probability, indicated that the match is not a random event. (2) All isotopically resolved peaks with intensities higher than 5% of the maximum intensity and m/z values above the m/z value of the selected precursor must match theoretical peptide fragments. (3) Manual interpretation of the fragment spectrum resulted in a continuous stretch of at least four amino acids. A sequence tag search with this stretch of amino acids must result in the same protein hit.

Cloning of human EYFP fusion proteins

Candidate genes selected from the screen after sequence analysis were amplified by PCR from commercially available cDNA clones from the German Resource Centre (RZPD, Berlin), from the National Institute of Technology and Evaluation (NITE, Chiba, Japan) or the Human cDNA Bank Section, Kazusa DNA Research Institute (Chiba, Japan) using sequence-specific sense and antisense primers (see supplementary material Table S2 for accession numbers). The full-length constructs were then cloned into pEYFP-C3 and pEYFP-N1 (Clontech). Authenticity of all constructs was verified by DNA sequencing.

Cell culture and transfection

HeLa CCL2 cells were grown in high glucose Dulbecco's modified Eagle's medium (DMEM; Invitrogen) supplemented with 10% foetal calf serum (FCS), 2 mM L-glutamine, 100 μg/ml penicillin and streptomycin at 37°C in a humidified 5% CO_2 incubator. Transient transfection of HeLa cells with plasmid DNA was performed with FuGENE 6 Transfection Reagent (Roche) following the manufacturer's recommendations.

Indirect immunofluorescence and imaging of fixed specimens

For immunofluorescence microscopy, HeLa cells grown on 0.01% poly-L-lysine-coated coverslips were fixed in methanol at –20°C or 3% paraformaldehyde in cytoskeletal buffer (300 mM NaCl, 10 mM sucrose, 10 mM $MgCl_2$, 20 mM PIPES pH 6.8) at 20°C, washed in PBS and blocked with PBS containing 10% FCS and 0.2% Triton X-100 for 30-60 minutes. The cells were incubated with primary antibodies for 60 minutes, or 15-30 minutes for EML3 antibodies (1:50 dilution of complete serum), washed three times in PBS, incubated for 60 minutes with secondary antibodies (anti-mouse or anti-guinea pig Cy3, Jackson Immuno Research, anti-mouse or anti-rabbit Alexa Fluor 488, Invitrogen) and finally washed again in PBS. Cells were then mounted on slides and DNA co-stained with DAPI (4,6-diamidino-2-phenylindole). Analysis and imaging was done with Deconvolution Leica DM IRE2 fluorescence microscope using the OpenLab software.

Production of transfected cell microarrays and time-lapse imaging

5 μl siRNA solution (30 μM), 3 μl Opti-MEM (Invitrogen) containing 0.4 M sucrose and 3.5 μl Lipofectamine 2000 (Invitrogen) were mixed and incubated for 20 minutes at room temperature. After incubation 7.25 μl of 0.2% gelatin and 0.00035% fibronectin (both Sigma-Aldrich) were added. 0.5 μl of a 40 μM marker solution of Cy3-labeled DNA oligonucleotide was added together with the siRNA to judge transfection efficiency. These final siRNA transfection cocktails were then arrayed onto single-well chambered LabTek coverglass live cell imaging dishes (NalgeNunc) using a ChipWriter Compact Robot (Bio-Rad) with solid pins (Point Technologies) resulting in a spot volume of ~4 nl (containing ~5 ng RNA) and a spot diameter of ~400 μm and a spot-to-spot distance of 1500 μm. siRNA microarrays were stored in plastic boxes containing silica gel (Merck) at least over night. After drying, 1.5 ml HeLa-H2B-EGFP cells (7.5×10^4 cells/ml) were plated on the microarrays in culture medium (DMEM containing 10% heat-inactivated foetal calf serum, 2 mM glutamine, 100 U/ml penicillin and 100 μg/ml streptomycin), and incubated for 29 hours at 37°C and 5% CO_2. Cells were transfected simply by growing on siRNA spots without further manipulation. After incubation for 29 hours, the 1.5 ml culture medium was removed and replaced with 5 ml preheated CO_2-independent imaging medium (Invitrogen) and live-cell microarrays were

transferred to the environmental microscope incubators. Time-lapse images of 30 minutes were acquired for 48 hours with an automated epifluorescence microscope (IX-81; Olympus-Europe) as described (Neumann et al., 2006).

Automated phenotyping by image processing

The image time series were analysed automatically as described (Neumann et al., 2006). The method classifies each cell nucleus in all image frames into predefined classes (interphase, mitosis, apoptosis, shape) and counts the overall proliferation rate. As a result, time curves of relative cell counts are obtained for each class. These curves are then smoothed to attenuate the influence of classification errors. For the negative controls (scrambled), mean and s.d. are calculated for each siRNA microarray, serving as siRNA microarray specific reference. For each siRNA, there were four replicates, resulting in four different time curves. To synthesise this information, the difference between experimental curves and control confidence band (control mean ± s.d.) was evaluated, resulting in a 'score' for each class and each siRNA. For the experimental data showing the most representative differences, time curves of different indices, still images and corresponding movies are presented.

Determination of mitotic indices and of metaphase chromatin extension

HeLa Kyoto cells were fixed and immunostained as described above. Condensation of chromatin and the appearance of microtubules served to determine the overall number of cells in mitosis and in the single mitotic stages, respectively. For Fig. 5B, the assembly of a correctly assembled spindle identified cells in metaphase, which were then investigated for regular alignment of all chromosomes. In Fig. 5C, the line of maximum chromatin extension in metaphase cells in a virtual pole-to-pole axis of the mitotic spindle was directly measured in the image (Adobe Photoshop TIFF files exported from OpenLab imaging software) and the absolute value determined using the magnification factor.

siRNA oligos

All siRNAs were synthetic double-stranded stealth select oligos (Invitrogen, Paisley, OR): We used oligos corresponding to the following ID numbers: FLJ46843/EML3: HSS137986 (1) and HSS137987 (2).

Quantitative RT-PCR

24 hours after transfection in 96-well plates, total RNA was extracted from HeLa Kyoto cells (Invisorb RNA extraction kit, Invitek), followed by reverse transcription reaction using TaqMan RT reagents (Applied Biosystems) and real-time qPCR using target-specific oligonucleotide primers (MWG) and SybrGreen PCR mastermix (Applied Biosystems) on an ABI 7500 system (Applied Biosystems). Calculating remaining target mRNAs relative to *GAPDH* mRNA, comparing siRNA-treated samples with scrambled control siRNA samples, assessed knockdown efficiency.

We thank Dirk Görlich, Bernd Bukau and Tony Hyman for antibodies against GFP, Hsc70 and OP18, respectively. We are grateful to Franz Herzog and Jan-Michael Peters for antibodies against human APC4 and APC7. We thank Iain Mattaj for help in the initial phase of the project. This work was supported by the ZMBH, University of Heidelberg. Many thanks to Eukaryon Biotech.

References

Acquaviva, C., Herzog, F., Kraft, C. and Pines, J. (2004). The anaphase promoting complex/cyclosome is recruited to centromeres by the spindle assembly checkpoint. *Nat. Cell Biol.* **6**, 892-898.

Askjaer, P., Galy, V., Hannak, E. and Mattaj, I. W. (2002). The Ran GTPase cycle and Importins alpha and beta are essential for spindle formation and nuclear envelope assembly in living Caenorhabditis elegans embryos. *Mol. Biol. Cell* **13**, 4355-4370.

Bamba, C., Bobinnec, Y., Fukuda, M. and Nishida, E. (2002). The GTPase Ran regulates chromosome positioning and nuclear envelope assembly in vivo. *Curr. Biol.* **12**, 503-507.

Bischoff, F. R., Maier, G., Tilz, G. and Ponstingl, H. (1990). A 47-kDa human nuclear protein recognized by antikinetochore autoimmune sera is homologous with the protein encoded by RCC1, a gene implicated in onset of chromosome condensation. *Proc. Natl. Acad. Sci. USA* **87**, 8617-8621.

Cassimeris, L. and Skibbens, R. V. (2003). Regulated assembly of the mitotic spindle: a perspective from two ends. *Curr. Issues Mol. Biol.* **5**, 99-112.

Catrein, I., Herrmann, R., Bosserhoff, A. and Ruppert, T. (2005). Experimental proof for a signal peptidase I like activity in Mycoplasma pneumoniae, but absence of a gene encoding a conserved bacterial type I SPase. *FEBS J.* **272**, 2892-2900.

Chen, Y., Kwon, S. W., Kim, S. C. and Zhao, Y. (2005). Integrated approach for manual evaluation of peptides identified by searching protein sequence databases with tandem mass spectra. *J. Proteome Res.* **4**, 998-1005.

Compton, D. A. (2000). Spindle assembly in animal cells. *Annu. Rev. Biochem.* **69**, 95-114.

Curmi, P. A., Gavet, O., Charbaut, E., Ozon, S., Lachkar-Colmerauer, S., Manceau, V., Siavoshian, S., Maucuer, A. and Sobel, A. (1999). Stathmin and its phosphoprotein family: general properties, biochemical and functional interaction with tubulin. *Cell Struct. Funct.* **24**, 345-357.

Dallol, A., Cooper, W. N., Al-Mulla, F., Agathanggelou, A., Maher, E. R. and Latif, F. (2007). Depletion of the Ras association domain family 1, isoform A-associated novel microtubule-associated protein, C19ORF5/MAP1S, causes mitotic abnormalities. *Cancer Res.* **67**, 492-500.

Dasso, M. (2002). The Ran GTPase: theme and variations. *Curr. Biol.* **12**, R502-R508.

Di Fiore, B., Ciciarello, M. and Lavia, P. (2004). Mitotic functions of the Ran GTPase network: the importance of being in the right place at the right time. *Cell Cycle* **3**, 305-313.

Dube, P., Herzog, F., Gieffers, C., Sander, B., Riedel, D., Muller, S. A., Engel, A., Peters, J. M. and Stark, H. (2005). Localization of the coactivator Cdh1 and the cullin subunit Apc2 in a cryo-electron microscopy model of vertebrate APC/C. *Mol. Cell* **20**, 867-879.

Eichenmuller, B., Everley, P., Palange, J., Lepley, D. and Suprenant, K. A. (2002). The human EMAP-like protein-70 (ELP70) is a microtubule destabilizer that localizes to the mitotic apparatus. *J. Biol. Chem.* **277**, 1301-1309.

Gadde, S. and Heald, R. (2004). Mechanisms and molecules of the mitotic spindle. *Curr. Biol.* **14**, R797-R805.

Gieffers, C., Peters, B. H., Kramer, E. R., Dotti, C. G. and Peters, J. M. (1999). Expression of the CDH1-associated form of the anaphase-promoting complex in postmitotic neurons. *Proc. Natl. Acad. Sci. USA* **96**, 11317-11322.

Gruss, O. J. and Vernos, I. (2004). The mechanism of spindle assembly: functions of Ran and its target TPX2. *J. Cell Biol.* **166**, 949-955.

Gruss, O. J., Wittmann, M., Yokoyama, H., Pepperkok, R., Kufer, T., Silljé, H., Karsenti, E., Mattaj, I. W. and Vernos, I. (2002). Chromosome-induced microtubule assembly mediated by TPX2 is required for spindle formation in HeLa cells. *Nat. Cell Biol.* **4**, 871-879.

Heidebrecht, H. J., Buck, F., Haas, K., Wacker, H. H. and Parwaresch, R. (1996). Monoclonal antibodies Ki-S3 and Ki-S5 yield new data on the 'Ki-67' proteins. *Cell Prolif.* **29**, 413-425.

Hetzer, M., Bilbao-Cortes, D., Walther, T. C., Gruss, O. J. and Mattaj, I. W. (2000). GTP hydrolysis by Ran is required for nuclear envelope assembly. *Mol. Cell* **5**, 1013-1024.

Hoepfner, S., Severin, F., Cabezas, A., Habermann, B., Runge, A., Gillooly, D., Stenmark, H. and Zerial, M. (2005). Modulation of receptor recycling and degradation by the endosomal kinesin KIF16B. *Cell* **121**, 437-450.

Houtman, S. H., Rutteman, M., De Zeeuw, C. I. and French, P. J. (2007). Echinoderm microtubule-associated protein like protein 4, a member of the echinoderm microtubule-associated protein family, stabilizes microtubules. *Neuroscience* **144**, 1373-1382.

Kline-Smith, S. L. and Walczak, C. E. (2004). Mitotic spindle assembly and chromosome segregation: refocusing on microtubule dynamics. *Mol. Cell* **15**, 317-327.

Kops, G. J., Weaver, B. A. and Cleveland, D. W. (2005). On the road to cancer: aneuploidy and the mitotic checkpoint. *Nat. Rev. Cancer* **5**, 773-785.

Kraft, C., Herzog, F., Gieffers, C., Mechtler, K., Hagting, A., Pines, J. and Peters, J. M. (2003). Mitotic regulation of the human anaphase-promoting complex by phosphorylation. *EMBO J.* **22**, 6598-6609.

Kraft, C., Gmachl, M. and Peters, J. M. (2006). Methods to measure ubiquitin-dependent proteolysis mediated by the anaphase-promoting complex. *Methods* **38**, 39-51.

Laemmli, U. K. (1970). Cleavage of structural proteins during the assembly of the head of bacteriophage T4. *Nature* **277**, 680-685.

Liska, A. J., Popov, A. V., Sunyaev, S., Coughlin, P., Habermann, B., Shevchenko, A., Bork, P. and Karsenti, E. (2004). Homology-based functional proteomics by mass spectrometry: application to the Xenopus microtubule-associated proteome. *Proteomics* **4**, 2707-2721.

Mack, G. J. and Compton, D. A. (2001). Analysis of mitotic microtubule-associated proteins using mass spectrometry identifies astrin, a spindle-associated protein. *Proc. Natl. Acad. Sci. USA* **98**, 14434-14439.

Mitchison, T. and Kirschner, M. (1984). Microtubule assembly nucleated by isolated centrosomes. *Nature* **312**, 232-237.

Neumann, B., Held, M., Liebel, U., Erfle, H., Rogers, P., Pepperkok, R. and Ellenberg, J. (2006). High-throughput RNAi screening by time-lapse imaging of live human cells. *Nat. Methods* **3**, 385-390.

Orban-Nemeth, Z., Simader, H., Badurek, S., Trancikova, A. and Propst, F. (2005). Microtubule-associated protein 1S, a short and ubiquitously expressed member of the microtubule-associated protein 1 family. *J. Biol. Chem.* **280**, 2257-2265.

Pollmann, M., Parwaresch, R., Adam-Klages, S., Kruse, M. L., Buck, F. and Heidebrecht, H. J. (2006). Human EML4, a novel member of the EMAP family, is essential for microtubule formation. *Exp. Cell Res.* **312**, 3241-3251.

Sauer, G., Korner, R., Hanisch, A., Ries, A., Nigg, E. A. and Sillje, H. H. (2005). Proteome analysis of the human mitotic spindle. *Mol. Cell. Proteomics* **4**, 35-43.

Sillje, H. H., Nagel, S., Korner, R. and Nigg, E. A. (2006). HURP is a Ran-importin beta-regulated protein that stabilizes kinetochore microtubules in the vicinity of chromosomes. *Curr. Biol.* **16**, 731-742.

Silverman-Gavrila, R. V. and Wilde, A. (2006). Ran is required before metaphase for spindle assembly and chromosome alignment and after metaphase for chromosome segregation and spindle midbody organization. *Mol. Biol. Cell* **17**, 2069-2080.

Suprenant, K. A., Dean, K., McKee, J. and Hake, S. (1993). EMAP, an echinoderm microtubule-associated protein found in microtubule-ribosome complexes. *J. Cell Sci.* **104**, 445-450.

Suprenant, K. A., Tuxhorn, J. A., Daggett, M. A., Ahrens, D. P., Hostetler, A., Palange, J. M., VanWinkle, C. E. and Livingston, B. T. (2000). Conservation of the WD-repeat, microtubule-binding protein, EMAP, in sea urchins, humans, and the nematode C. elegans. *Dev. Genes Evol.* **210**, 2-10.

Topper, L. M., Campbell, M. S., Tugendreich, S., Daum, J. R., Burke, D. J., Hieter, P. and Gorbsky, G. J. (2002). The dephosphorylated form of the anaphase-promoting complex protein Cdc27/Apc3 concentrates on kinetochores and chromosome arms in mitosis. *Cell Cycle* **1**, 282-292.

Wittmann, T., Hyman, A. and Desai, A. (2001). The spindle: a dynamic assembly of microtubules and motors. *Nat. Cell Biol.* **3**, E28-E34.